PAPER

Check for updates

Enhancing electrocatalytic CO$_2$ reduction *via* engineering substrate–cluster interaction†

Qian Sun,[a] Huiru Yang,*[a] Chunmei Zhang [iD] *[ac] and Aijun Du [iD] [b]

Cu clusters exhibit exceptional performance in the electrocatalytic carbon dioxide reduction reaction (CO$_2$RR) due to their tunable size. Using first-principles calculations, we systematically investigate the CO$_2$RR on small Cu$_n$ clusters (n = 3, 8, 13) anchored on a T′-WTe$_2$ substrate, denoted as Cu$_n$@T′-WTe$_2$. Given that the hydrogen evolution reaction (HER) often competes with the CO$_2$RR, we further investigated the competition between the CO$_2$RR and HER. Our results show that Cu$_n$@T′-WTe$_2$ outperforms pure Cu$_n$ clusters as catalysts, with enhanced CO$_2$RR activity. The CO$_2$RR performance of Cu$_n$@T′-WTe$_2$ enhances with increasing cluster size, and surpasses the HER activity in Cu$_{13}$@T′-WTe$_2$. This enhancement stems from the substrate–cluster interactions, where the buckled ''non-uniform surface'' of T′-WTe$_2$ deforms the larger Cu$_{13}$ cluster, optimizing the CO$_2$RR efficiency. We propose a potential strategy for WTe$_2$-supported Cu clusters to boost CO$_2$RR while suppressing HER by leveraging substrate-supported Cu clusters.

1. Introduction

The accumulation of greenhouse gases, particularly carbon dioxide (CO$_2$), drives global warming and poses significant environmental and energy challenges.[1,2] To address rising energy demands and mitigate CO$_2$ emissions, researchers have explored various strategies to convert CO$_2$ into valuable chemicals and feedstocks,[3] including chemical reforming,[4,5] bioconversion,[6] photocatalysis,[7,8] and electrocatalysis.[9,10] Among them, the electrochemical CO$_2$ reduction reaction (CO$_2$RR) stands out as a promising approach, transforming CO$_2$ into valuable products[8,10–12] like methane (CH$_4$),[6,13] formic acid (HCOOH),[14] and methanol (CH$_3$OH).[15,16] However, the CO$_2$RR faces challenges such as low efficiency and poor product selectivity[4,9,17] exacerbated by the competing hydrogen evolution reaction (HER), which significantly reduces the performance of the CO$_2$RR.[18]

To overcome these limitations, significant efforts have focused on designing efficient electrocatalysts that activate inert CO$_2$ molecules while suppressing the competitive HER. Various systems, including metals,[19,20] metal oxides,[21,22] clusters,[23] carbon-based materials,[24,25] and metal–organic frameworks,[26,27] have been explored. Among them, clusters, in particular Cu clusters, demonstrate excellent CO$_2$RR catalytic performance.[28,29] When supported on substrates, the synergistic interaction between the substrate and cluster significantly influences the CO$_2$RR efficiency.[30] Thus, optimizing the substrate–cluster pairing is critical to maximizing the CO$_2$RR activity and minimizing HER interference.

In this study, we employ first-principles calculations to examine the CO$_2$RR performance of Cu$_n$ clusters (n = 3, 8, 13) anchored on a T′-WTe$_2$ substrate denoted as Cu$_n$@WTe$_2$.[31–33] Compared to unsupported Cu$_n$ (Cu$_3$, Cu$_8$, and Cu$_{13}$),[28,34–36] our findings reveal that the T′-WTe$_2$ substrate reduces the absolute limiting potential for the CO$_2$RR process ($|U_L|$),[37] while inhibiting the competitive HER. This improvement is attributed to the strong distortion of larger Cu$_{13}$ clusters by the buckled T′-WTe$_2$ surface, facilitating rapid charge transfer between the cluster and substrate. Our work provides an effective approach for enhancing CO$_2$RR efficiency *via* engineering substrate–cluster interactions.

2. Computational methods

Spin-polarized density functional theory (DFT) calculations were carried out using the Vienna ab initio simulation package (VASP).[38,39] The projector-augmented-wave (PAW) method was employed to treat the core wave functions.[40] The generalized gradient approximation (GGA) in the Perdew–Burke–Ernzerhof (PBE) form is adopted.[41,42] Long-range van der Waals (vdW) interaction was corrected using the DFT-D3 scheme,[43] and a vacuum space exceeding 20 Å was used to minimize periodic interactions. The 3 × 3 × 1 Monkhorst–Pack k-points in the Brillouin zone are sampled for structural optimizations, and

[a] School of Physics, Northwest University, Xi'an 710127, China.
  E-mail: y1573349346@163.com, chunmeizhang@nwu.edu.cn
[b] School of Chemistry and Physics and QUT Center for Materials Science,
  Queensland University of Technology (QUT), Brisbane, QLD 4000, Australia
[c] Shaanxi Key Laboratory for Theoretical Physics Frontiers, Xi'an 710127, China
† Electronic supplementary information (ESI) available. See DOI: https://doi.org/10.1039/d5cp01541c

dense $6 \times 6 \times 1$ k-meshes are set for the density of states (DOS) calculations for T′-WTe$_2$. 15 Å $\times$ 15 Å $\times$ 15 Å cubic cells are used to optimize the isolated Cu$_3$, Cu$_8$ and Cu$_{13}$ clusters before loading on the WTe$_2$ surfaces. The cutoff energy for the plane wave basis is 400 eV in all the calculations, and the energy and force convergence criterion are respectively set to 10^{-5} eV and 10^{-2} eV Å^{-1}. We used VASPsol for the implicit solvation calculations.[44] Water is considered as the continuum solvent throughout, with a bulk static dielectric constant ε_s of 80.[45] In addition, canonical *ab initio* molecular dynamics simulations (AIMDs) with a Nosé thermostat and integrating time with the Verlet algorithm at a time step of 1 fs are employed to investigate the thermodynamic stability of the catalyst.[46]

The isolated CO$_2$ molecule is simulated in a large cubic cell of 15 Å in length. The adsorption energies are calculated according to the equation $E_{ads} = E_{adsorbed\text{-}system} - E_{molecule} - E_{catalyst}$, where $E_{adsorbed\text{-}system}$, $E_{molecule}$, and $E_{catalyst}$ are the total energies of the catalyst with CO$_2$*, the isolates CO$_2$ molecule and Cu$_n$@WTe$_2$ (n = 3, 8, 13), respectively. The Bader charge, charge density difference, and DOS are calculated to clarify the interactions between the adsorbed molecule and the catalyst surface. To calculate the free energy profiles of the electrocatalytic CO$_2$RR, the computational electrode model (CHE) is employed.[47] The free energy change (ΔG) at each elementary step of the CO$_2$RR process is calculated using the equation $\Delta G = \Delta E + \Delta ZPE - T\Delta S$, where ΔE is the total energy change

calculated by DFT, ΔZPE is the zero-point energy correction through frequency analysis, and T and ΔS are the reaction temperature (T = 298.15 K) and the entropy value change, respectively. The limiting potential (U_L) is defined as the maximum free energy change using the relation $U_L = -\Delta G_{PDS}/e$, where ΔG_{PDS} is the maximum free energy increase in a potential determining step (PDS). In addition, we utilized the post-processing functionalities provided by qvasp and VASPKIT to analyze the computational results.[48]

For isolated Cu$_n$ clusters, our calculations show finite magnetic moments ($1\mu_B$ for Cu$_3$, $0\mu_B$ for Cu$_8$, and $5\mu_B$ for Cu$_{13}$), in line with previous data.[49,50] However, when supported on the T′-WTe$_2$ substrate, the whole system becomes nonmagnetic. The charge transfer between the clusters and substrate fully quenches the magnetism.

3. Results and discussion

3.1. Structural models of Cu$_n$ (n = 3, 8, 13) clusters, CO$_2$ adsorption on Cu$_n$ and CO$_2$RR on Cu$_n$

The most stable structures of Cu$_3$, Cu$_8$, and Cu$_{13}$ are an equilateral triangle geometry with C_{2v} symmetry,[34] a tetragonal crystal with D_{2d} symmetry,[36] and an icosahedron geometry with I_h symmetry (see Fig. 1a–c),[35,51] respectively. The calculated Cu–Cu bond lengths (L_{Cu-Cu}) are 2.34 Å for Cu$_3$, 2.30–2.50 Å for Cu$_8$, and 2.53 Å for Cu$_{13}$, which agree well with previously reported values.[36,49,50,52]

We first examine CO$_2$ adsorption on Cu$_n$ (n = 3, 8, 13) clusters. The most stable adsorption configurations are depicted in Fig. 1d–f, revealing a bent CO$_2$ geometry on all Cu$_n$ clusters, which indicates effective activation of the CO$_2$ molecule. For the CO$_2$RR, CH$_4$ is the sole product across all cluster sizes; however, the potential-determining step (PDS) varies with cluster size, and the overpotential increases as the cluster size grows (see Table 1). The calculated free energy profile and the corresponding reaction intermediates along the most favorable CO$_2$RR pathway are provided in the ESI† (see Fig. S1 and S2). Additionally, we further investigate the HER on the Cu$_n$ cluster (Fig. 1g–i). A comparison of U_L between CO$_2$RR and HER, presented in Table 1, shows that the HER suppresses the CO$_2$RR on all pure Cu$_n$ clusters (see Fig. S13, ESI†).

3.2. Geometric structures of T′-WTe$_2$

To investigate whether substrate selection can enhance CO$_2$RR performance, we build on our prior findings identifying T′-WTe$_2$ as an effective substrate that could interact with clusters
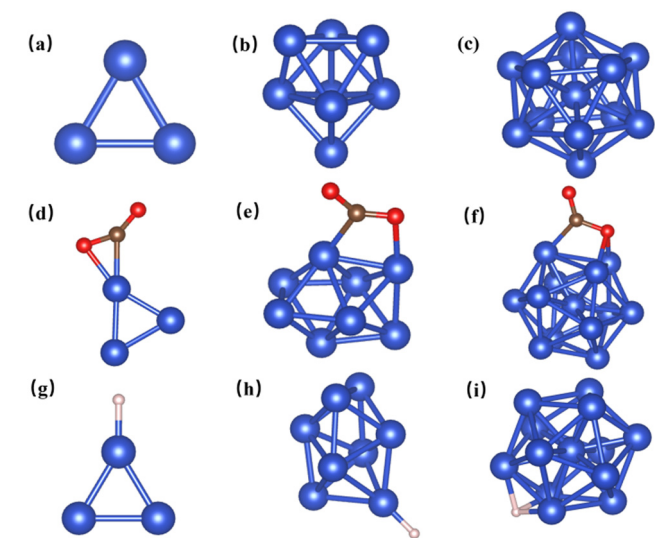

Fig. 1 (a)–(c) Structures of the pristine Cu$_3$, Cu$_8$ and Cu$_{13}$ clusters. (d)–(f) The most stable adsorption configurations for CO$_2$ on Cu$_3$, Cu$_8$, and Cu$_{13}$ clusters. (g)–(i) The optimized configurations for H adsorption on Cu$_3$, Cu$_8$, and Cu$_{13}$.

Table 1 Calculated PDS and U_L and the final product of the CO$_2$RR with Cu$_n$ (n = 3, 8, 13) catalysts in contrast to the HER

| Configurations | CO$_2$RR | | | HER |
	PDS	U_L (V)	Product	U_L (V)
Cu$_3$	*CO + e$^-$ + H$^+$ → *CHO	0.64	CH$_4$	−0.51
Cu$_8$	*OCHOH + e$^-$ + H$^+$ → *CHO + H$_2$O	0.85	CH$_4$	0.73
Cu$_{13}$	*CO + e$^-$ + H$^+$ → *CHO	0.89	CH$_4$	−0.14

This journal is © the Owner Societies 2025

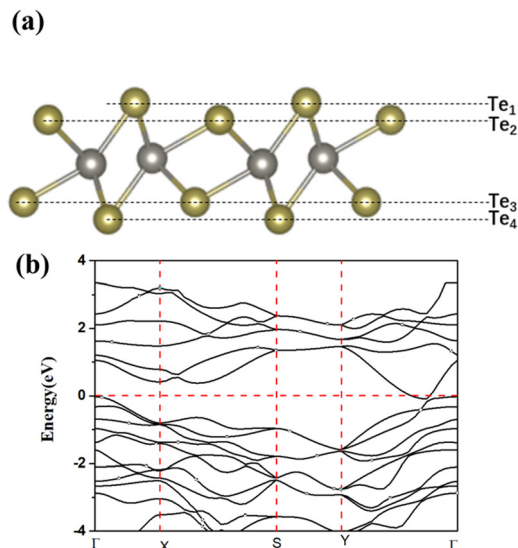*Phys. Chem. Chem. Phys.*, 2025, **27**, 12190–12197 | **12191**

Fig. 2 (a) Schematic of the 3×2 supercell of T′-WTe$_2$. W and Te atoms are denoted by grey and orange spheres, respectively. (b) Band structure for the T′-WTe$_2$ monolayer.

sufficiently.[30,53] Consequently, we selected T′-WTe$_2$ as the substrate for loading clusters to further evaluate its CO$_2$RR properties.

The monoclinic metal T′ phase of WTe$_2$, a semimetal with no band gap (Fig. 2b), was synthesized decades ago (Fig. 2a),[32] a characteristic corroborated by the calculated partial density of states (PDOS) in Fig. S6 (ESI†). T′-WTe$_2$ features three atomic layers, with nonequivalent top (Te$_1$ and Te$_2$) and bottom (Te$_3$ and Te$_4$) Te layers. The Te$_1$ atom sits higher than Te$_2$ in

the top layer, forming what we term as a 'nonuniform surface',[33] with bond lengths of 2.72 Å ($L_{Te_2–W}$) and 2.83 Å ($L_{Te_1–W}$).

3.3. CO$_2$ adsorption and electroreduction for Cu$_n$@T′-WTe$_2$ (n = 3, 8, 13)

Firstly, we investigate the adsorption of Cu$_n$ (n = 3, 8, 13) clusters on the T′-WTe$_2$ substrate, with all optimized configurations presented in Fig. S3–S5 (ESI†). The most stable structures for Cu$_3$@T′-WTe$_2$ (Fig. S3b, ESI†), Cu$_8$@T′-WTe$_2$ (Fig. S4h, ESI†), and Cu$_{13}$@T′-WTe$_2$ (Fig. S5d, ESI†) are highlighted, in Fig. 3 for further studying the CO$_2$RR. Bader charge analysis (Table S1, ESI†) reveals electron transfers of 0.28e, 0.32e and 0.18e from Cu$_3$, Cu$_8$, and Cu$_{13}$ to T′-WTe$_2$, respectively, indicating significant substrate–cluster interactions, further evidenced by orbital hybridization in the PDOS (Fig. S7, ESI†). As noted in Section 2, while isolated Cu$_n$ clusters exhibit size-dependent magnetism, the interaction with the T′-WTe$_2$ substrate leads to complete spin quenching. The AIMD simulation at 500 K over 5ps (Fig. S11, ESI†) shows no structural degradation, confirming the excellent thermal stability of the Cu$_n$@T′-WTe$_2$ catalyst under ambient conditions.

To assess the substrate's role in the CO$_2$RR performance, we studied CO$_2$ adsorption on the Cu$_3$@T′-WTe$_2$, Cu$_8$@T′-WTe$_2$, and Cu$_{13}$@T′-WTe$_2$ surfaces. Various adsorption configurations of CO$_2$ on the catalyst surfaces are considered as shown in Fig. S8 (ESI†). Strong adsorption energy typically elongates the C–O bond length in the adsorbed CO$_2$ molecule.[17,54,55] Fig. 3 presents the most favorable sites for CO$_2$ adsorption, showing $L_{C–O}$ extended to 1.22 Å and 1.88 Å (Fig. 3a), 1.25 Å and 1.28 Å (Fig. 3d), and 1.26 Å (Fig. 3g) for the Cu$_3$@T′-WTe$_2$,
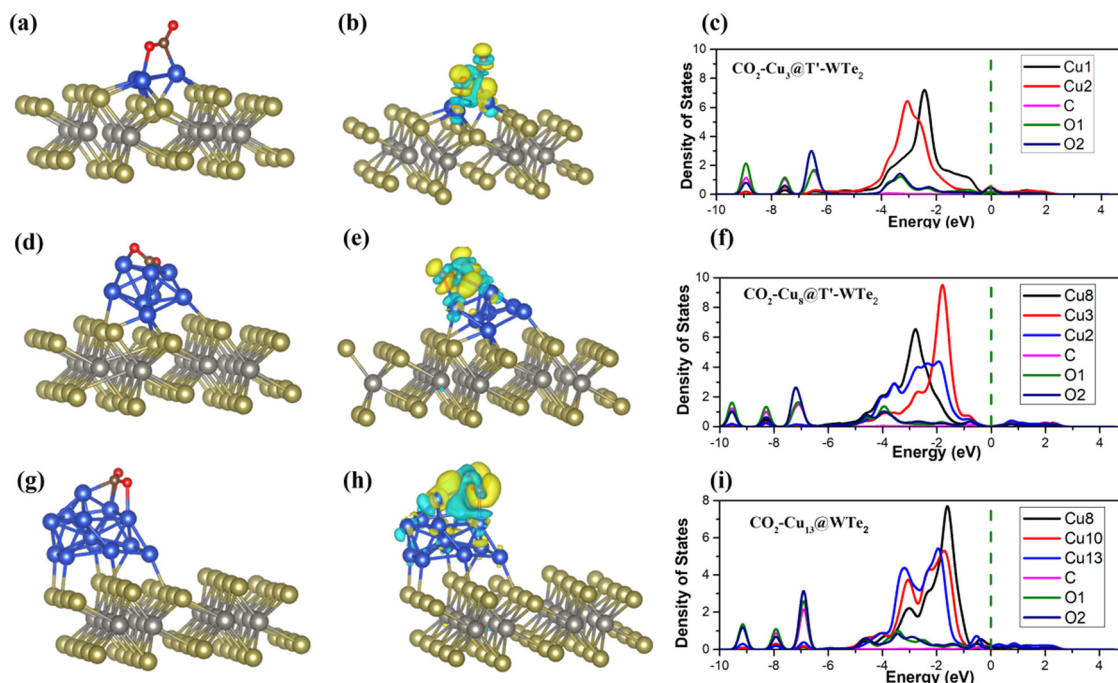

Fig. 3 The most stable adsorption configurations, the isosurface of the charge density difference with an isovalue of 0.003 Å^{-1}, and the PDOS for CO$_2$ on Cu$_3$@WTe$_2$: (a)–(c), Cu$_8$@WTe$_2$ (d)–(f) and Cu$_{13}$@WTe$_2$ (g)–(i). The blue (yellow) wireframes denote the loss (gain) of electrons with the isosurface values set as 0.003 Å^{-3}. The Fermi level is assigned at 0 eV.

12192 | *Phys. Chem. Chem. Phys.*, 2025, **27**, 12190–12197

This journal is © the Owner Societies 2025

Table 2 Parameters of adsorbed CO_2 on the Cu_n@WTe_2 (n = 3, 8, 13). Including adsorption free energies ($E_{ads\text{-}free}$), O=C=O angles ($\angle OCO$), the corresponding C=O bond lengths ($L_{C=O}$) of Cu_n@WTe_2 (n = 3, 8, 13), and the net charge transferred from adsorbents to CO_2 (Δq is calculated based on the Bader charges)

Adsorption configurations	$E_{ads\text{-}free}$ (eV)	$\angle OCO$	L_{C-O} (Å)	Δq (e)
CO_2–Cu_3@WTe_2	−0.10	134.2°	1.22; 1.28	0.62
CO_2–Cu_8@WTe_2	−0.33	130.6°	1.25; 1.28	0.79
CO_2–Cu_{13}@WTe_2	0.02	132.3°	1.26	0.74

Cu_8@T′-WTe_2 and Cu_{13}@T′-WTe_2 systems, respectively, suggesting enhanced activation of CO_2. After CO_2 adsorption, the linear O=C=O geometry bends into a V-shape, with the ($\angle OCO$ angles decreasing from 179.9° to 134.2° for Cu_3@WTe_2) (Table 2). Similarly, the same trend can be observed for Cu_8@WTe_2 and Cu_{13}@WTe_2, indicating effective CO_2 activation by Cu_n@WTe_2. The PDOS analysis shown in Fig. 3c, f, and i

reveals orbital hybridization and charge transfer between Cu, C, and O atoms, underscoring the strong interaction between the CO_2 molecules and the Cu_n@T′-WTe_2 catalysts.[11,56,57] The charge density difference (see Fig. 3) and the Bader charge analysis (Table 2) further confirm electron donation from Cu_n@WTe_2 to the CO_2 molecule (around 0.62e–0.79e). The broadly dispersed PDOS peaks for C and O relative to isolated CO_2 molecules (Fig. S9, ESI†) and the hybridization with Cu atoms also support the strong interaction between CO_2 and Cu_n.

3.4. CO_2 reduction reaction pathways on the Cu_n@WTe_2 (n = 3, 8, 13)

We next explore the CO_2RR pathways on Cu_n@WTe_2. Fig. 4 illustrates the calculated free energy profile for the most favorable CO_2RR pathways on Cu_3@WTe_2, Cu_8@WTe_2, and Cu_{13}@WTe_2, with the corresponding optimal reaction configurations shown in Fig. S10 (ESI†). For CO_2–Cu_3@WTe_2, the
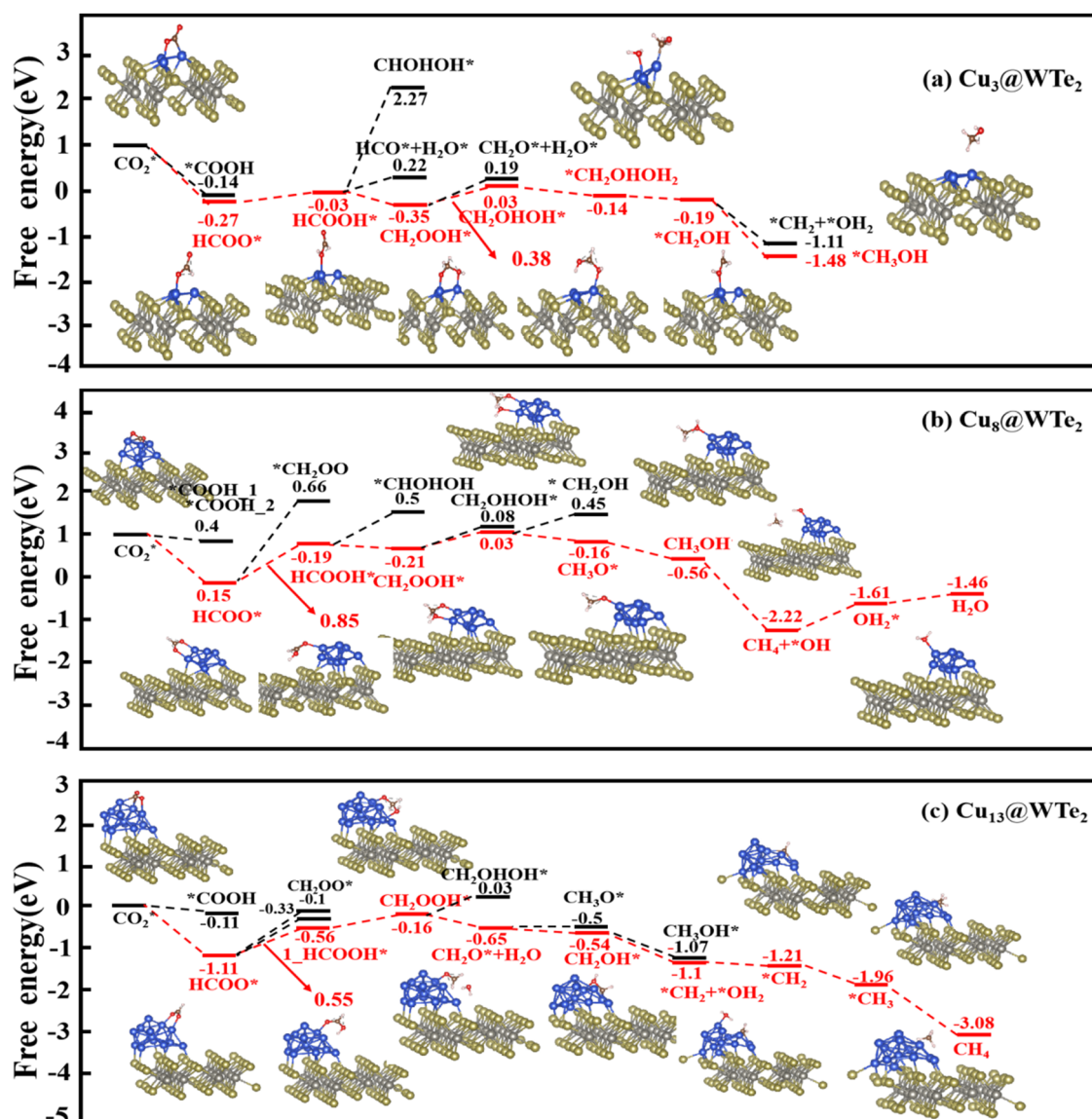
Fig. 4 Free energy diagram for the electrochemical CO_2RR on (a) Cu_3@WTe_2, (b) Cu_8@WTe_2, and (c) Cu_{13}@WTe_2.

This journal is © the Owner Societies 2025

Phys. Chem. Chem. Phys., 2025, **27**, 12190–12197 | **12193**

Table 3 The calculated U_L ($|U_L|$), HCOO intermediate adsorption ($\Delta G_{HCOO}*$) and final product of CO_2RR, and the H* intermediate adsorption (ΔG_H*) of the HER with $Cu_n@WTe_2$ ($n = 3, 8, 13$) catalysts

	CO₂RR			HER	
Configurations	$\|U_L\|$ (V)	$\Delta G_{HCOO}*$ (eV)	Product	$\|U_L\|$ (V)	ΔG_H* (eV)
$Cu_3@WTe_2$	0.38	−0.27	CH_3OH	0.10	0.10
$Cu_8@WTe_2$	0.86	−1.04	CH_4	0.05	−0.05
$Cu_{13}@WTe_2$	0.55	−1.11	CH_4	0.85	−0.85

initial H^+ and e^- pair attacks the carbon atom of CO_2, forming HCOO* with a free energy change of −0.27 eV. Subsequent hydrogenation yields HCOOH*, followed by an exothermic step forming CH_2OOH* as shown in Fig. 4a, which is energetically more preferred than the formation of CHOHOH* or HCO* + H_2O*. Further hydrogenation of CH_2OOH* favors CH_2OHOH* ($\Delta G < 0$) over $CH_2O* + H_2O*$. Two subsequent additions of the H^+ and e^- pair will attack the O atom, releasing the H_2O molecule and leaving $*CH_2OH$, which undergoes successive hydrogenation steps to produce CH_3OH molecules. Overall, the PDS is the formation of CH_2OHOH* from CH_2OOH* with a U_L of −0.38 V.

For the $Cu_8@WTe_2$ and $Cu_{13}@WTe_2$ surface, the initial step of the CO_2RR is the formation of HCOO*, followed by hydrogenation of HCOO* to form HCOOH* (see Fig. 4b and c), which is more energetically favorable than that of CH_2OO*. HCOOH* then converts to CH_2OOH*. On $Cu_8@WTe_2$, CH_2OOH* after hydrogenation will transform into $CH_2O* + *OH_2$, proceeding to CH_3OH* and ultimately producing CH_4. On $Cu_{13}@WTe_2$, CH_2OOH will be further hydrogenated to CH_2O* with H_2O release, followed by hydrogenation to $*CH_4$ with the final release of the CH_4 molecule. The PDS for both the $Cu_8@WTe_2$ and $Cu_{13}@WTe_2$ systems is HCOO* → HCOOH*, with U_L values of −0.85 V and −0.55 V, respectively. The free energy values ($G(T)$) for these pathways are detailed in Table S3 (ESI†).

The analysis reveals that $Cu_3@WTe_2$, $Cu_8@WTe_2$, and $Cu_{13}@WTe_2$ all exhibit robust CO_2RR activity. On $Cu_3@WTe_2$, CO_2RR proceeds via a $6e^-$ charge transfer pathway, yielding CH_3OH, whereas $Cu_8@WTe_2$ and $Cu_{13}@WTe_2$ favor an $8e^-$ charge transfer reaction pathway, producing CH_4 as the primary product. Comparison of the overpotentials with pure Cu_n clusters (Table S2, ESI†) shows that Cu_n on the T′-WTe₂ substrate outperforms their standalone counterparts, with lower $|U_L|$ values indicating enhanced CO_2RR efficiency. Specifically, $|U_L|$ for $Cu_3@WTe_2$ is 0.38 V (vs. 0.64 V for pure Cu_3, a 0.26 V reduction), while $|U_L|$ for $Cu_{13}@WTe_2$ is 0.55 V (vs. 0.89 V for pure Cu_{13}, a 0.34 V reduction). This suggests that the T′-WTe₂ substrate significantly boosts the CO_2RR performance, with the enhancement scaling with Cu cluster size.

3.5. Analysis of the hydrogen evolution reaction and solvent effects

To evaluate the competing HER,[18] we analyzed the HER performance on $Cu_n@WTe_2$ ($n = 3, 8, 13$), as detailed in Fig S12 and S14 (ESI†). In all the optimized configurations, H atoms preferentially bind to Cu clusters rather than the WTe₂ surface.

Catalytic selectivity was assessed using the difference in U_L values, i.e., $|U_{L(CO_2)}| - |U_{L(H_2)}|$,[37] where a positive value of $|U_{L(CO_2)}| - |U_{L(H_2)}|$ indicates a poor CO_2RR selectivity over the HER. For the $Cu_{13}@T′\text{-}WTe_2$, the $|U_{L(CO_2)}| - |U_{L(H_2)}|$ is calculated to be −0.30 V (see Table 3), suggesting a better CO_2RR selectivity over the HER. Given that HCOO* is a critical intermediate in all CO_2RR pathways, we then considered the competition between H* and HCOO*.[55,58–60] For the $Cu_{13}@WTe_2$, HCOO* formation (Fig. 4c) has a free energy change of −1.11 eV, more favorable than −0.85 eV for the HER process (see Table 3), indicating greater HCOO* stability over H*.

To further gain an in-depth understanding of the catalyst effects, we compared the DOS curves of isolated and adsorbed HCOO* intermediates on the catalyst. As shown in Fig S15 (ESI†), the 2p orbitals of O and C atoms after adsorption shift toward lower energy region near the Fermi level, with larger shifts reflecting stronger intermediate–substrate interaction, and the lower adsorption energy.[17,61,62] $Cu_{13}@WTe_2$ exhibits the lowest adsorption energy (−1.11 eV) compared to −0.27 eV for $Cu_3@WTe_2$. This suggests that the buckled T′-WTe₂ surface enhances CO_2RR activity in the supported Cu_n nanocluster, with larger cluster size strengthening substrate–Cu interactions and boosting electrocatalytic CO_2 reduction.

Overall, $Cu_{13}@WTe_2$ emerges as the optimal CO_2RR electrocatalyst among the studied configurations. We further examine its electrochemical CO_2RR performance using free energy diagrams with an implicit solvation model (Fig. S16, ESI†). The PDS remains unchanged, with the U_L value shifting by only 0.09 V upon incorporating the solvation effect. These findings suggest that the electrolyte environment exerts minimal influence on the CO_2RR performance of the $Cu_{13}@WTe_2$ catalysts.

4. Conclusions

In conclusion, we theoretically investigate the CO_2 electrocatalytic properties on pure Cu clusters and their performance when supported on a T′-WTe₂ substrate. Our results reveal that the introduction of the WTe₂ substrate significantly reduces the CO_2RR overpotential across the system, with $Cu_{13}@WTe_2$ exhibiting particularly notable suppression of the competing hydrogen evolution reaction (HER). Our findings elucidate the size-dependent electrocatalytic behavior of the CO_2RR and HER across different Cu clusters while highlighting the critical role of the substrate in modulating electrochemical performance. Collectively, this work offers valuable insights and a strategic framework for designing efficient CO_2RR catalysts, paving the way for future experimental advancement in electrocatalytic systems.

Author contributions

Qian Sun: data curation, writing – original draft. Huiru Yang: revise the manuscript. Chunmei Zhang: writing – original draft, writing – review & editing. Aijun Du: revise the manuscript and

12194 | *Phys. Chem. Chem. Phys.*, 2025, **27**, 12190–12197

This journal is © the Owner Societies 2025

technical support. All authors contributed to the results interpretation and manuscript preparation.

Data availability

The data presented in this work is available from the corresponding author upon reasonable request.

Conflicts of interest

There is no conflict to declare.

References

1 Y. Shi, M. Chen and F. Wang, In Research on energy-saving of the pebble thermoregulation greenhouse, Global Conference on Civil, Structural and Environmental Engineering/3rd International Symp on Multi-field Coupling Theory of Rock and Soil Media and its Applications, China Three Gorges Univ, Yichang, PEOPLES R CHINA, 2012, Oct 20–21, China Three Gorges Univ, Yichang, PEOPLES R CHINA, 2012, pp. 2112–2115.

2 Y. Shi and M. Chen, In Study on temperature distribution regularity of pebble thermoregulation greenhouse, Global Conference on Civil, Structural and Environmental Engineering/3rd International Symp on Multi-field Coupling Theory of Rock and Soil Media and its Applications, China Three Gorges Univ, Yichang, PEOPLES R CHINA, 2012 Oct 20–21, China Three Gorges Univ, Yichang, PEOPLES R CHINA, 2012, pp. 2116–2119.

3 D. J. D. Pimlott, A. Jewlal, Y. Kim and C. P. Berlinguette, Oxygen-Resistant CO_2 Reduction Enabled by Electrolysis of Liquid Feedstocks, J. Am. Chem. Soc., 2023, 145(48), 25933–25937.

4 Y. Zhang, In On Study of Teaching Reform of Organic Chemistry Course in Applied Chemical Industry Technology, 2017 3rd International Conference on Energy, Environment and Materials Science (EEMS), Northwestern Polytechnical University, Singapore, SINGAPORE, 2017 Jul 28–30, Northwestern Polytechnical University, Singapore, SINGAPORE, 2017.

5 G. Liu, X. Mao, B. Yang, J. Shang and Z. Wu, Research progress on chemical looping reforming of macromolecular components of volatiles from biomass pyrolysis based on decoupling strategy, Fuel Process. Technol., 2022, 235, 107375.

6 S. Fu, I. Angelidaki and Y. Zhang, In situ Biogas Upgrading by CO_2-to-CH_4 Bioconversion, Trends Biotechnol., 2021, 39(4), 336–347.

7 M. Shen, L. Zhang and J. Shi, Defect Engineering of Photocatalysts towards Elevated CO2 Reduction Performance, ChemSusChem, 2021, 14(15), 3226.

8 X. Feng, Y. Pi, Y. Song, C. Brzezinski, Z. Xu, Z. Li and W. Lin, Metal-Organic Frameworks Significantly Enhance Photocatalytic Hydrogen Evolution and CO_2 Reduction with Earth-Abundant Copper Photosensitizers, J. Am. Chem. Soc., 2020, 142(2), 690–695.

9 A. R. Woldu, Z. Huang, P. Zhao, L. Hu and D. Astruc, Electrochemical CO_2 reduction (CO_2RR) to multi-carbon products over copper-based catalysts, Coord. Chem. Rev., 2022, 454, 214340.

10 Z.-Y. Du, K. Wang, S.-B. Li, Y.-M. Xie, J.-H. Tian, Q.-N. Zheng, W. F. Ip, H. Zhang, J.-F. Li and Z.-Q. Tian, In Situ Raman Spectroscopic Studies of Electrochemical CO_2 Reduction on Cu-Based Electrodes, J. Phys. Chem. C, 2024, 128(28), 11741–11755.

11 Z. Zhao, Z. Chen, X. Zhang and G. Lu, Generalized Surface Coordination Number as an Activity Descriptor for CO_2 Reduction on Cu Surfaces, J. Phys. Chem. C, 2016, 120(49), 28125–28130.

12 T. Liu, G. Song, X. Liu, Z. Chen, Y. Shen, Q. Wang, Z. Peng and G. Wang, Insights into the mechanism in electrochemical CO_2 reduction over single-atom copper alloy catalysts: A DFT study, Iscience, 2023, 26(10), 107953.

13 H. Dong, Y. Li and D.-E. Jiang, First-Principles Insight into Electrocatalytic Reduction of CO_2 to CH_4 on a Copper Nanoparticle, J. Phys. Chem. C, 2018, 122(21), 11392–11398.

14 M. Rozenberg, A. Loewenschuss and C. J. Nielsen, H-Bonding of Formic Acid with Its Decomposition Products: A Matrix Isolation and Computational Study of the HCOOH/CO and HCOOH/CO_2 Complexes, J. Phys. Chem. A, 2015, 119(31), 8497–8502.

15 S. Xue, X. Liang, Q. Zhang, X. Ren, L. Gao, T. Ma, A. Liu and I. A. Pasti, Density Functional Theory Study of CuAg Bimetal Electrocatalyst for CO_2RR to Produce CH_3OH, Catalysts, 2024, 14(1), 7.

16 C. Christophe, Silica-supported PdGa Nanoparticles: Metal Synergy for Highly Active and Selective CO2-to-CH3OH Hydrogenation, JACS Au, 2022, 2(8), 1946–1947.

17 P. Saha, S. Amanullah and A. Dey, Selectivity in Electrochemical CO_2 Reduction, Acc. Chem. Res., 2022, 55(2), 134–144.

18 C. Kim, J. Kim, S. Joo, Y. Yang, J. Shin, M. Liu, J. Cho and G. Kim, Highly Efficient CO_2 Utilization via Aqueous Zinc- or Aluminum- CO_2 Systems for Hydrogen Gas Evolution and Electricity Production, Angew. Chem., Int. Ed., 2019, 58(28), 9506–9511.

19 J. Gao, H. Wang, K. Feng, C. Xiang, H. Wang, H. Qi, Y. Liu, H. Tian, J. Zhong and Z. Kang, Cu atomic clusters on N-doped porous carbon with tunable oxidation state for the highly-selective electroreduction of CO2, Mater. Adv., 2020, 1(7), 2286–2292.

20 H. Xie, T. Wang, J. Liang, Q. Li and S. Sun, Cu-based nanocatalysts for electrochemical reduction of CO_2, Nano Today, 2018, 21, 41–54.

21 Y. Xia, Q. Zhang, F. Guo, J. Wang, W. Li and J. Xu, Ag@Cu with Cu-CuO interface prepared by air cold-plasma promoting the electrocatalytic reduction of CO_2 to low-carbon alcohols, Vacuum, 2022, 196, 110767.

22 S. Choe, J. Kim, S. Y. Kim and S. H. Ahn, Controlling the surface oxidation state of halogenated Cu-based catalyst for electrochemical reduction of carbon dioxide to ethylene, J. Alloys Compd., 2024, 1005.

This journal is © the Owner Societies 2025

Phys. Chem. Chem. Phys., 2025, 27, 12190–12197 | 12195

23 X.-X. Li, L. Zhang, J. Liu, L. Yuan, T. Wang, J.-Y. Wang, L.-Z. Dong, K. Huang and Y.-Q. Lan, Design of Crystalline Reduction-Oxidation Cluster-Based Catalysts for Artificial Photosynthesis, *JACS Au*, 2021, **1**(8), 1288–1295.

24 Y. Gao, M. Zhao, L. Jiang and Q. Yu, Electrochemical CO_2 reduction of graphene single-atom/cluster catalysts, *Mol. Catal.*, 2024, **562**, 114225.

25 S.-Y. Wu, T.-C. Chuang and H.-T. Chen, Electrochemical CO_2 reduction on Single-Atom aluminum catalysts supported on graphene and N-doped Graphene: Mechanistic insights and hydration effects, *Appl. Surf. Sci.*, 2025, **681**, 161523.

26 E. Plaza-Mayoral, V. Okatenko, K. N. Dalby, H. Falsig, I. Chorkendorff, P. Sebastian-Pascual and M. Escudero-Escribano, Composition effects of electrodeposited Cu-Ag nanostructured electrocatalysts for CO_2 2 reduction, *Iscience*, 2024, **27**(6), 109933.

27 X.-G. Zhang, S. Feng, C. Zhan, D.-Y. Wu, Y. Zhao and Z.-Q. Tian, Electroreduction Reaction Mechanism of Carbon Dioxide to C_2 Products via Cu/Au Bimetallic Catalysis: A Theoretical Prediction, *J. Phys. Chem. Lett.*, 2020, **11**(16), 6593–6599.

28 D. Gao, S. Rao, Y. Li, N. Liu and D. Wang, Enhancement of CO adsorption energy on defective graphene-supported Cu_{13} cluster and prediction with an induction energy model, *Appl. Surf. Sci.*, 2023, **615**, 156368.

29 A. Y. Ermilov, A. V. Soloviev, Y. N. Morosov and T. I. Shabatina, Interaction of Copper Clusters with Dioxidine, *Moscow Univ. Chem. Bull.*, 2024, **79**(4), 233–238.

30 H. Yang, W. Zou, C. Zhang and A. Du, Ab Initio Studies of Electrocatalytic CO_2 Reduction for Small Cu Cluster Supported on Polar Substrates, *ACS Appl. Mater. Interfaces*, 2024, **16**(26), 33688–33695.

31 C. Huang, A. Narayan, E. Zhang, Y. Liu, X. Yan, J. Wang, C. Zhang, W. Wang, T. Zhou, C. Yi, S. Liu, J. Ling, H. Zhang, R. Liu, R. Sankar, F. Chou, Y. Wang, Y. Shi, K. T. Law, S. Sanvito, P. Zhou, Z. Han and F. Xiu, Inducing Strong Superconductivity in WTe_2 by a Proximity Effect, *ACS Nano*, 2018, **12**(7), 7185–7196.

32 P. Zhang, P. Li, Q. Ma, M. Shen, Z. Tian and Y. Liu, Interfacial properties of In-plane monolayer 2H-$MoTe_2$/1T? -WTe_2 heterostructures, *Appl. Surf. Sci.*, 2023, **623**, 157022.

33 Y. Maximenko, Y. Chang, G. Chen, M. R. Hirsbrunner, W. Swiech, T. L. Hughes, L. K. Wagner and V. Madhavan, Nanoscale studies of electric field effects on monolayer 1T′-WTe_2, *Npj Quant. Mater.*, 2022, **7**(1), 29.

34 V. E. Matulis, O. A. Ivashkevich and V. S. Gurin, DFT study of electronic structure and geometry of anionic copper clusters, *J. Mol. Struct. Theochem.*, 2004, **681**(1–3), 169–176.

35 Q. Zeng, X. Wang, M. L. Yang and H. B. Fu, Interplay between geometrical and electronic stability of neutral and anionic Cu_{13} clusters: a first-principles study, *Eur. Phys. J.*, 2010, **58**(1), 125–129.

36 C. A. Barboza, A. Gambetta, R. Arratia-Perez, P. L. Rodriguez-Kessler, A. Munoz-Castro and D. MacLeod-Carey, Structural, electronic and magnetic properties of copper(I) cubic clusters, *Polyhedron*, 2021, **195**, 114878.

37 G. Henkelman, B. P. Uberuaga and H. Jónsson, A climbing image nudged elastic band method for finding saddle points and minimum energy paths, *J. Chem. Phys.*, 2000, **113**(22), 9901–9904.

38 K. Furthmuller, Efficient iterative schemes for ab initio total-energy calculations using a plane-wave basis set, *Phys. Rev. B: Condens. Matter Mater. Phys.*, 1996, **54**(16), 11169–11186.

39 J. Hafner, Ab-initio simulations of materials using VASP:: Density-functional theory and beyond, *J. Comput. Chem.*, 2008, **29**(13), 2044–2078.

40 K. Burke, J. P. Perdew and M. Levy, Improving energies by using exact electron densities, *Phys. Rev. A: At., Mol., Opt. Phys.*, 1996, **53**(5), R2915–R2917.

41 X. Xu and W. A. Goddard, The extended Perdew-Burke-Ernzerhof functional with improved accuracy for thermodynamic and electronic properties of mazular systems, *J. Chem. Phys.*, 2004, **121**(9), 4068–4082.

42 P. E. Blöchl, Projector augmented-wave method, *Phys. Rev. B: Condens. Matter Mater. Phys.*, 1994, **50**(24), 17953–17979.

43 S. Grimme, J. Antony, S. Ehrlich and H. Krieg, A consistent and accurate ab initio parametrization of density functional dispersion correction (DFT-D) for the 94 elements H-Pu, *J. Chem. Phys.*, 2010, **132**(15), 154104.

44 H. S. Lee and M. E. Tuckerman, Ab initio molecular dynamics with discrete variable representation basis sets: Techniques and application to liquid water, *J. Phys. Chem. A*, 2006, **110**(16), 5549–5560.

45 G. Fisicaro, L. Genovese, O. Andreussi, N. Marzari and S. Goedecker, A generalized Poisson and Poisson-Boltzmann solver for electrostatic environments, *J. Chem. Phys.*, 2016, **144**(1), 014103.

46 A. Lahanas and V. Tsaoussidis, Exploiting the efficiency and fairness potential of AIMD-based congestion avoidance and control, *Comput. Networks*, 2003, **43**(2), 227–245.

47 J. K. Nørskov, J. Rossmeisl, A. Logadottir, L. Lindqvist, J. R. Kitchin, T. Bligaard and H. Jónsson, Origin of the Overpotential for Oxygen Reduction at a Fuel-Cell Cathode, *J. Phys. Chem. B*, 2004, **108**(46), 17886–17892.

48 V. Wang, N. Xu, J.-C. Liu, G. Tang and W.-T. Geng, VASPKIT: A user-friendly interface facilitating high-throughput computing and analysis using VASP code, *Comput. Phys. Commun.*, 2021, **267**, 108033.

49 G. Guzman-Ramirez, F. Aguilera-Granja and J. Robles, DFT study of the fragmentation channels and electronic properties of Cu_n^{ν} ($\nu = \pm 1, 0, 2$; n = 3-13) clusters, *Eur. Phys. J. D*, 2010, **57**(3), 335–342.

50 V. L. Mazalova, A. V. Soldatov, S. Adam, A. Yakovlev, T. Moeller and R. L. Johnston, Small Copper Clusters in Ar Shells: A Study of Local Structure, *J. Phys. Chem. C*, 2009, **113**(21), 9086–9091.

51 V. E. Matulis, D. M. Palagin, A. S. Mazheika and O. A. Ivashkevich, DFT study of electronic structure and geometry of anionic copper clusters Cu_n^- (n = 11, 12, 13), *J. Mol. Struct. Theochem.*, 2008, **857**(1–3), 66–71.

52 E. E. Karagiannis, C. E. Kefalidis, I. Petrakopoulou and C. A. Tsipis, Density Functional Study of Structural,

12196 | *Phys. Chem. Chem. Phys.*, 2025, **27**, 12190–12197

This journal is © the Owner Societies 2025

Electronic, and Optical Properties of Small Bimetallic Ruthenium-Copper Clusters, *J. Comput. Chem.*, 2011, **32**(7), 1241–1261.

53 H. Yang, W. Zou, K. Ostrikov, C. Zhang and A. Du, Tuning electrocatalytic nitrogen reduction on supported nickel cluster via substrate phase engineering, *Appl. Surf. Sci.*, 2023, **640**, 158277.

54 Y. Gao, X. Tu, X. Liu, Y. Zhang, M. Huang, J. Zhu and H. Jiang, Advances in DFT study of electronic structure and geometry of anionic copper clusters CO_2 Electroreduction over Hollow Fiber Gas Diffusion Electrodes, *ChemCatChem*, 2024, **16**, 17.

55 M. Hu, L. Li, J. Li, K. Zahra and Z. Zhang, Two-dimensional Cu-based materials for electrocatalytic carbon dioxide reduction, *Iscience*, 2024, **27**(3), 109313.

56 W. Choi, Y. Chae, E. Liu, D. Kim, W. S. Drisdell, H.-S. Oh, J. H. Koh, D. K. Lee, U. Lee and D. H. Won, Exploring the influence of cell configurations on Cu catalyst reconstruction during CO2 electroreduction, *Nat. Commun.*, 2024, **15**(1), 8345.

57 W. Nie, G. P. Heim, N. B. Watkins, T. Agapie and J. C. Peters, Organic Additive-derived Films on Cu Electrodes Promote Electrochemical CO2 Reduction to C2+ Products Under Strongly Acidic Conditions, *Angew. Chem., Int. Ed.*, 2023, **62**(12), 202216102.

58 C. Christophe, Silica-supported PdGa Nanoparticles: Metal Synergy for Highly Active and Selective CO2-to-CH3OH Hydrogenation, *JACS Au*, 2021, **2**(8), 1946–1947.

59 Q. Xu, J. Jiang, X. Sheng, Q. Jing, X. Wang, L. Duan and H. Guo, Understanding the synergistic effect of piezoelectric polarization and the extra electrons contributed by oxygen vacancies on an efficient piezo-photocatalysis CO_2 reduction, *Inorg. Chem. Front.*, 2023, **10**(10), 2939–2950.

60 R. Cai, M. Sun, J. Ren, M. Ju, X. Long, B. Huang and S. Yang, Unexpected high selectivity for acetate formation from CO_2 reduction with copper based 2D hybrid catalysts at ultralow potentials, *Chem. Sci.*, 2021, **12**(46), 15382–15388.

61 O. F. Lopes and H. Varela, Effect of Annealing Treatment on Electrocatalytic Properties of Copper Electrodes toward Enhanced CO_2 Reduction, *ChemistrySelect*, 2018, **3**(31), 9046–9055.

62 Q. Chang, J. H. Lee, Y. Liu, Z. Xie, S. Hwang, N. S. Marinkovic, A.-H. A. Park, S. Kattel and J. G. Chen, Electrochemical CO_2 Reduction Reaction over Cu Nanoparticles with Tunable Activity and Selectivity Mediated by Functional Groups in Polymeric Binder, *Jacs Au*, 2022, **2**(1), 214–222.

This journal is © the Owner Societies 2025

Phys. Chem. Chem. Phys., 2025, **27**, 12190–12197 | **12197**